ELSEVIER

Journal of Structural Geology 29 (2007) 1872–1881

JOURNAL OF STRUCTURAL GEOLOGY

www.elsevier.com/locate/jsg

Effect of mica on the grain size of dynamically recrystallized quartz in a quartz–muscovite mylonite

Won Joon Song, Jin-Han Ree*

Department of Earth and Environmental Sciences, Korea University, Seoul 136-701, South Korea

Received 27 June 2007; received in revised form 15 September 2007; accepted 19 September 2007
Available online 7 October 2007

Abstract

Quartz ribbons in a quartz–muscovite mylonite from the Sunchang shear zone of South Korea show a variation in the average size (25–107 μm) of dynamically recrystallized quartz depending on the fraction and dispersion of muscovite within the ribbons. Micas within the quartz ribbons occur both inside quartz grains and along their boundaries, having a strong preferred orientation with the basal planes parallel to the mylonitic foliation. Micas (or mica aggregates) inside the quartz show a size range of 1–25 μm, whereas those along the quartz grain boundaries range from 2 to 98 μm. The average quartz grain size (D) calculated from three-dimensional grain size distribution decreases drastically with increasing mica volume fraction (F_m) up to $F_m = 3\%$ in the ribbons, and further increases in the mica fractions above 3% result in only a little decrease (with some fluctuation) in the quartz grain size, generating the equation of $D = -20.11 \times \ln F_m - 9.64$. With almost the same fraction of mica however, the quartz ribbons with dispersed mica show a smaller quartz grain size than those with clustered mica, indicating the importance of dispersion as well as fraction of second-phase particles to the grain size of dynamically recrystallized quartz. Quartz c-axes tend to have a random orientation with an $F_m > 3\%$, presumably due to the greater contribution to the total deformation of grain boundary sliding for quartz with a smaller grain size ($D < 47$ μm).

Keywords: Quartz–muscovite mylonite; Dynamic recrystallization; Grain size; Second-phase particles; Particle dispersion; Deformation mechanism

1. Introduction

Second-phase particles are important for the dynamic recrystallization processes of a main phase, as they inhibit grain boundary migration (thus dynamic grain growth) of the main phase and stabilize the grain size below steady-state recrystallized grain size (e.g. Olgaard, 1990; Krabbendam et al., 2003; Herwegh and Berger, 2004). With a reduced grain size, the dominant deformation mechanism of the main phase can switch from grain-size insensitive dislocation creep to grain-size sensitive diffusion creep (e.g. Etheridge and Wilkie, 1979; De Bresser et al., 1998, 2001). Despite the importance of the effect of second phase, there have only been a few studies on the effect of second-phase particles on recrystallization of the main phase in geologic materials; the effect of mica on the grain size of recrystallized calcite in static heating experiments (Olgaard and Evans, 1986, 1988) and natural carbonate mylonite (Herwegh and Jenni, 2001; Herwegh and Berger, 2004; Herwegh et al., 2005), the effects of dolomite and silicate minerals on the grain size of statically recrystallized calcite in natural marble (Mas and Crowley, 1996), the effect of mica on the grain size of statically recrystallized quartz in natural metacherts (Masuda et al., 1991), and the effect of graphite on dynamically recrystallized quartz in natural quartz mylonite (Krabbendam et al., 2003). Furthermore, there has been no study on the influence of mica on the dynamic recrystallization of quartz, even though quartz–mica mylonites and mica-bearing metapsammites are common in continental deformation belts. In this paper, we report the effects of mica fraction and dispersion on the dynamic recrystallization of quartz in the quartz ribbons of a quartz–muscovite mylonite.

* Corresponding author. Tel.: +82 2 3290 3175; fax: +82 2 3290 3189.
E-mail address: reejh@korea.ac.kr (J.-H. Ree).

0191-8141/$ - see front matter © 2007 Elsevier Ltd. All rights reserved.
doi:10.1016/j.jsg.2007.09.011

We also suggest that the dominant deformation mechanism can switch from dislocation creep to grain-size sensitive creep with increasing mica fraction.

2. Geological setting

Samples of quartz–muscovite mylonite were collected from the Osanri Formation of the late Paleozoic Pyeongan Supergroup within the Sunchang shear zone, which is a southwestern branch of the Honam shear zone system (Fig. 1; Cluzel et al., 1991; Kim and Kee, 1994). The Middle Jurassic Honam shear zone is a right-lateral strike-slip shear zone with a northeast trend, which played an important role in the Mesozoic tectonic evolution of the Korean peninsula (Yanai et al., 1985; Cluzel et al., 1991; Ree and Hwang, 1994; Ree et al., 2001; Sagong et al., 2005). The current erosion level of the Honam shear zone, in general, is shallower toward the northeast, resulting in different temperature conditions of the cropped-out rocks in the shear zone (Cluzel et al., 1991). In the Yecheon shear zone, a northeastern branch of the Honam shear zone system, for example, the main shearing occurred under middle greenschist-facies conditions, with a deformation temperature between 335 and 355 °C, where quartz grains were deformed by dislocation creep with subgrain rotation recrystallization or under Regime 2 of Hirth and Tullis (1992), while feldspar porphyroclasts were deformed mainly by cataclasis (Ree et al., 2005; Park et al., 2006). In the Sunchang shear zone of the southwestern Honam shear zone system, quartz grains of mylonites were deformed by dislocation creep with combined grain boundary migration and subgrain rotation recrystallization or under Regime 3 of Hirth and Tullis (1992), as shown in more detail in the following section. In granitic mylonites of the Sunchang shear zone, almost all feldspar grains, showing a wide range of grain size (0.05–2 mm), have very thin mechanical twins and kink bands, with some grains carrying deformation bands. The feldspar grains show either sweeping or patchy undulatory extinction, with the rare occurrence of subgrains. Many feldspar grains also exhibit intragranular fractures with little displacement along the fractures. Some boundaries between feldspar grains are serrated. These feldspar microstructures are similar to those of the transition from zone 3 to zone 2 of Pryer (1993), suggesting a deformation temperature between 400 and 450 °C.

3. Microfabrics of quartz–muscovite mylonite

The quartz–muscovite mylonite examined in this study is composed of quartz ribbons embedded in a muscovite-rich matrix (Fig. 2). The matrix consists mostly of muscovite (>95%), with minor contents of quartz (3–4%), biotite

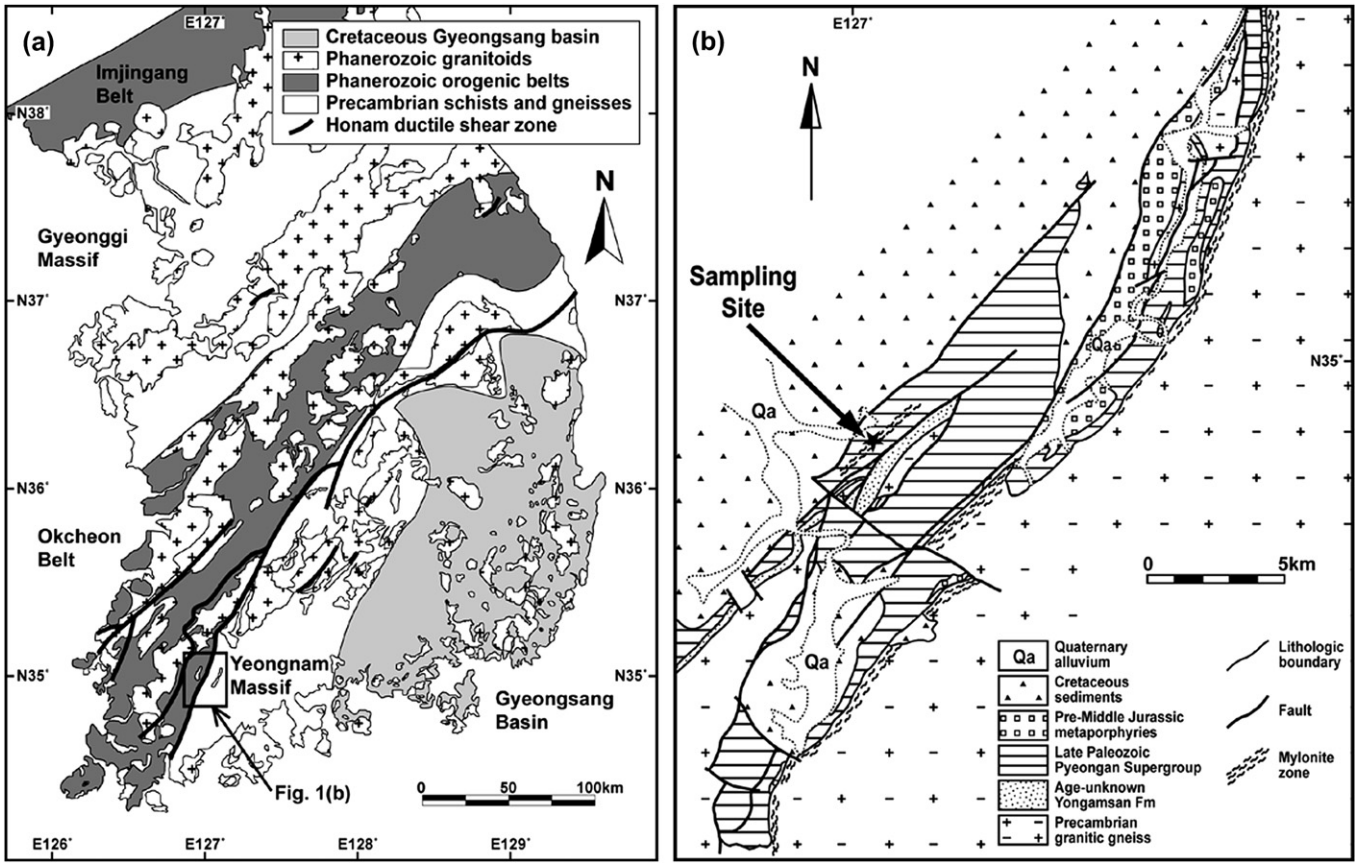

Fig. 1. (a) Geologic map of the southern Korean peninsula. (b) Geologic map around the Sunchang shear zone in Hwasun area. Modified after Kim and Kee (1994).

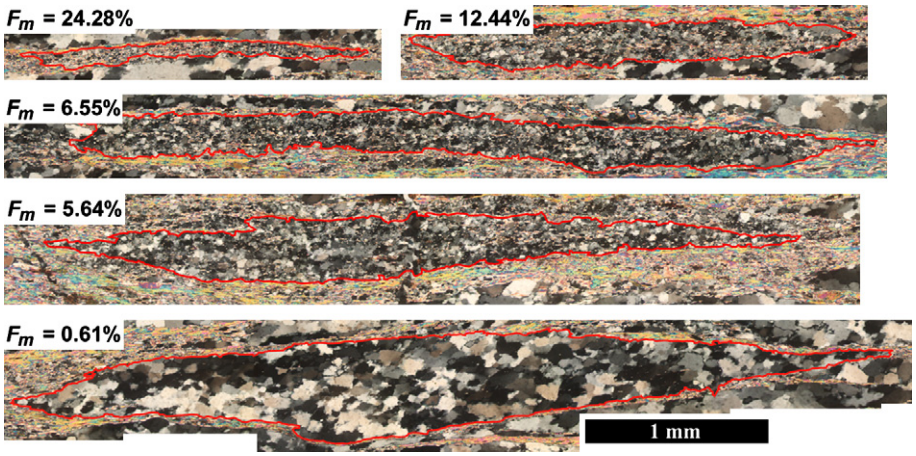

Fig. 2. Photomicrographs of quartz ribbons (outlined by red line) in the quartz–muscovite mylonite. F_m: area fraction of muscovite within the ribbons. Both upper and lower polarizers were rotated 45° counterclockwise.

(<1%), opaques (<1%) and retrograde chlorite (<1%). The mylonitic foliation is defined by a preferred orientation of muscovites and flattened-cigar-shaped quartz ribbons, with the lineation defined by a preferred orientation of quartz ribbons on the foliation surface. The flattened-cigar-shaped quartz ribbons have an average axial ratio of 1:3.9:15.5, with a long dimension between 0.9 and 9.1 mm. The quartz ribbons contain fine-grained muscovite particles, with their volume fractions ranging from 0.47 to 24.28% (Fig. 2). The size of quartz grains decreases with increasing fraction of muscovite particles, which will be shown in detail in the following section. The muscovite particles occur as individual grains or aggregates within the ribbons, and show undulose extinction and kink bands. The muscovite particles or aggregates can be divided into 'inclusion' muscovites within the quartz grains and 'boundary' muscovites along the quartz grain boundaries. The sizes of the inclusion muscovites range from 1 to 25 μm, while those of the boundary muscovites range from 2 to 98 μm. The ratio of the boundary to inclusion micas tends to increase from 1.5 to 14.5 with increasing mica fraction within the quartz ribbons.

Since the size of many muscovite grains are smaller than the thickness (~10 μm) of our ultra-thin section, the muscovite area fraction measured in the thin section in transmitted light is not true volume fraction. To obtain the true volume fraction of muscovite from photomicrographs in transmitted light, we used a line-slicing method by Krabbendam et al. (2003). Hereafter, mica fraction represents mica volume fraction.

The quartz grains in the ribbons with a mica fraction of less than 3% show sweeping undulose extinction, wavy or lobate grain boundaries, deformation bands and subgrains (Fig. 3a). The subgrains of quartz are either equiaxed or tabular. The larger, tabular subgrains have straight subgrain boundaries at a high angle to the mylonitic foliation. The quartz grains in the ribbons with a mica fraction of more than 3% also show

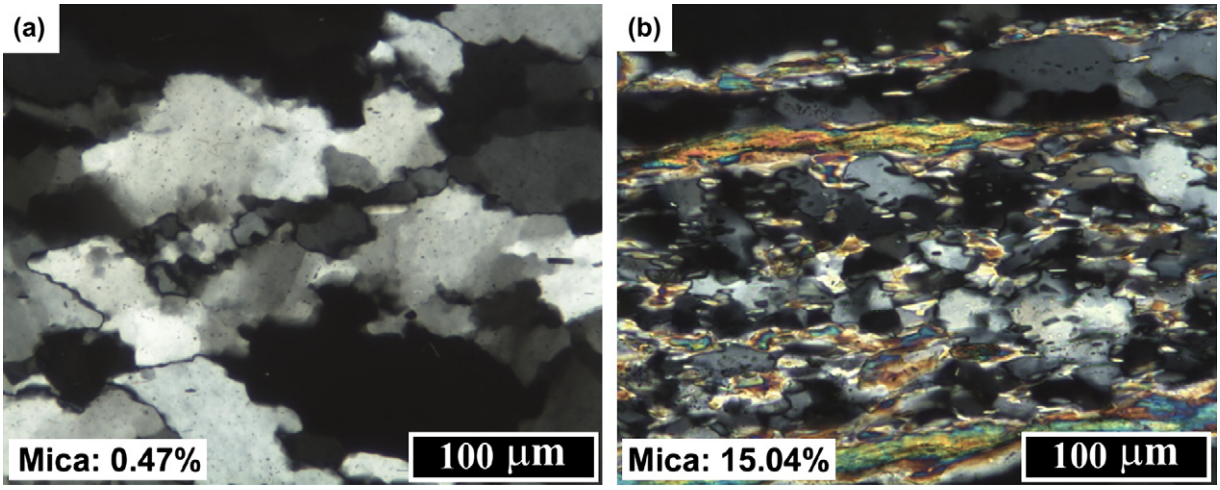

Fig. 3. (a) Photomicrograph of quartz microstructure in almost pure quartz ribbon. (b) Photomicrograph of quartz microstructure in quartz ribbon with mica fraction of 15.04%. Crossed-polarized light. Both upper and lower polarizers were rotated 45° counterclockwise in (b).

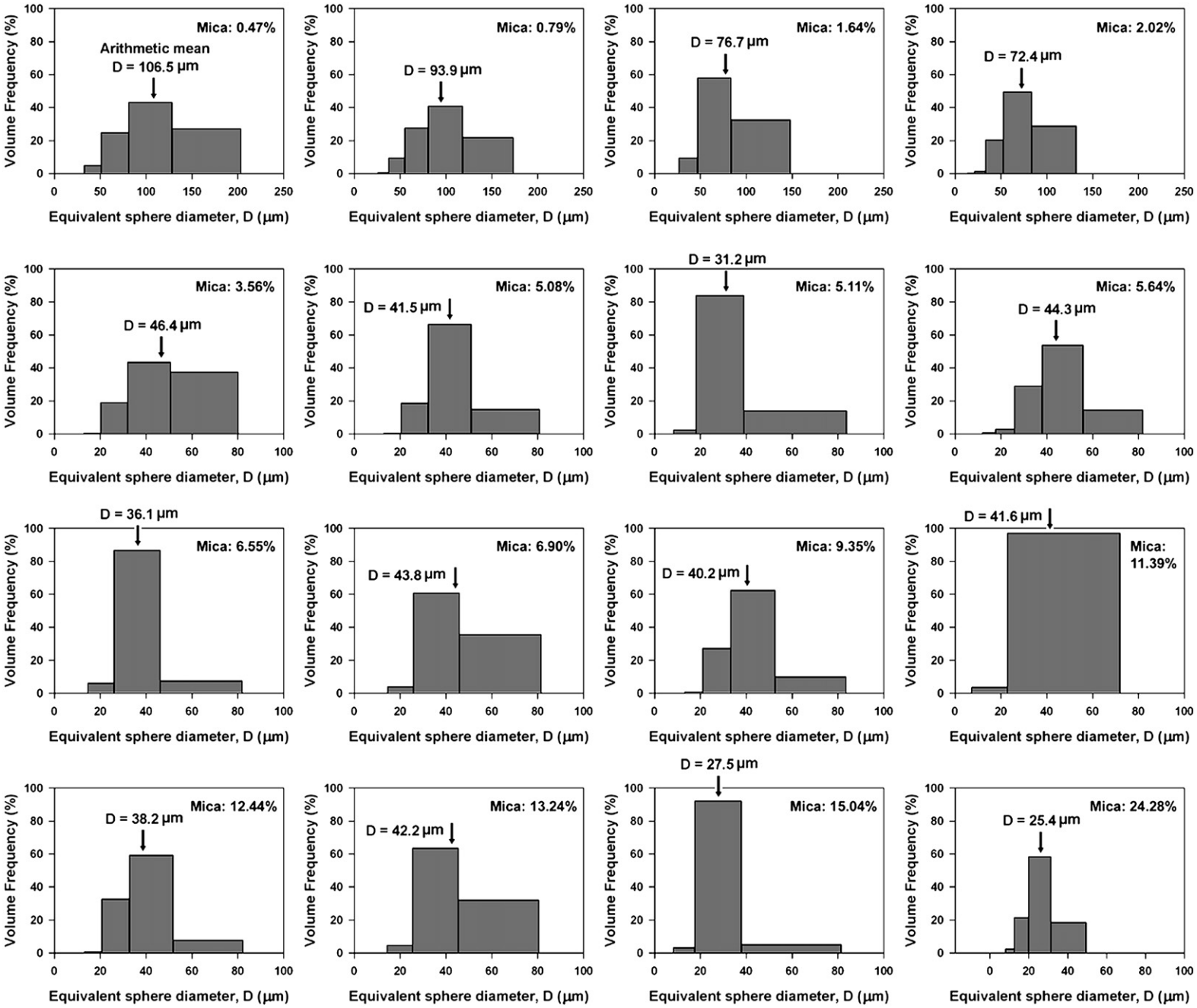

Fig. 4. 3D volumetric distribution of quartz grains with varying mica fraction in the quartz ribbons. The size bins are logarithmic.

sweeping undulose extinction, but most of the grain boundaries are slightly wavy or straight and subgrains are rare (Fig. 3b and also see Fig. 6).

The axial ratio of the quartz grains within the ribbons with a mica fraction of less than 20% on a section cut perpendicular to the foliation and parallel to the lineation (*b*-section) is about the same (1.4–1.6) as that on a section cut perpendicular to the lineation (*a*-section), with their long axis oblique to the mylonitic foliation on the *b*-section. With a mica fraction of more than 20%, the axial ratio of the quartz grains on the *b*-section tends to be higher (up to 2.0), presumably due to anisotropic grain growth as explained by Herwegh and Berger (2004).

3.1. Grain size analysis of quartz

3.1.1. Methods

For the analysis of the grain size distribution, the 3D volumetric distribution (volume fraction per size class) was used because the frequency distribution (number of grains per size class) does not appropriately reflect the physical significance of the 3D grain size distribution (Heilbronner and Bruhn, 1998). Here, the grain size of elongated quartz is defined as the diameter of a sphere with the same volume as an ellipsoidal grain.

For the grain size measurement, the grain boundaries of quartz were manually traced on transparencies using optical photomicrographs of the ultra-thin section and AVA (Achsenverteilungsanalyse; Sander, 1970) diagrams constructed from an automated fabric analyzer apparatus developed at the University of Melbourne (Russell-Head and Wilson, 2001; Wilson et al., 2003). After scanning the transparent overlays with the grain boundary traces, the scanned images were converted into binary images using the CorelDraw™11 software. The 2D cross-sectional area of each grain was measured using the public domain software ImageJ (http://rsb.info.nih.gov/ij/). The average 3D axial ratio of the grains was obtained using Panozzo's (1983, 1984) method, for both *a*- and *b*-sections. The cross-sectional length of the long axis of individual grains was calculated using the 2D cross-sectional area of each grain obtained from the ImageJ and the average axial ratio of the grains on the *b*-section, assuming individual grains to have an ellipsoidal shape with parallel long axes.

The 3D grain volume distribution was obtained using the CSDCorrections 1.37 software (Higgins, 2000, 2006), with input data including the cross-sectional length of the long axis of individual grains, the average 3D aspect ratio of the grains and the total area occupied by the grains. For ellipsoidal grains, the CSDCorrections software generates the volume fraction per size (longaxis) class after incorporating the cut-section and intersection probability effects (Higgins, 2000, 2006). From this 3D volume distribution, the arithmetic mean of the long axis of the grains and the volume of the average ellipsoidal grain were calculated using the average axial ratio of the grains. Finally, to represent the average grain size, the average volume of the ellipsoidal grains was converted to the diameter of an equivalent sphere.

3.1.2. Results

The 3D volumetric distribution of quartz grains with varying mica fractions within the quartz ribbons is shown in Fig. 4. The size bins in Fig. 4 are logarithmic, as the logarithmic size bins simplify the calculations for the conversion of 2D into 3D grain sizes (Higgins, 2000, 2006). The mean size of quartz grains markedly decreases even with a small increase in the mica fraction, up to a mica fraction of about 3% (Fig. 5; Table 1). In contrast, a further increase in the mica fraction above 3% results in a slight decrease in the quartz grain size. The relationship between the mica fraction and quartz grain size can be represented by

$$D = -20.11 \times \ln F_m - 9.64 \quad (1)$$

where D is the mean size of the quartz grains and F_m is the mica volume fraction, although there are some large deviations in the quartz grain size from this best-fit curve, particularly for quartz ribbons with mica fraction of more than 3% (Fig. 5). For example, the quartz ribbon with a mica fraction of 6.55% has a mean quartz grain size (36.1 μm) larger than that (31.2 μm) with a mica fraction of 5.11% (Fig. 6). This deviation is presumably due to the effect of particle dispersion. A quartz ribbon with more mica can have quartz grains larger than that with less mica if the mica grains are more clustered in the former. The effect of second-phase particle dispersion will be discussed later.

The quartz grain size determined by the linear intercept method is also shown in Fig. 5. For the linear intercept method, the line-intercepts were counted both parallel and normal to the mylonitic foliation on the *b*-section and the mean intercept length is multiplied by 1.5 for conversion to the

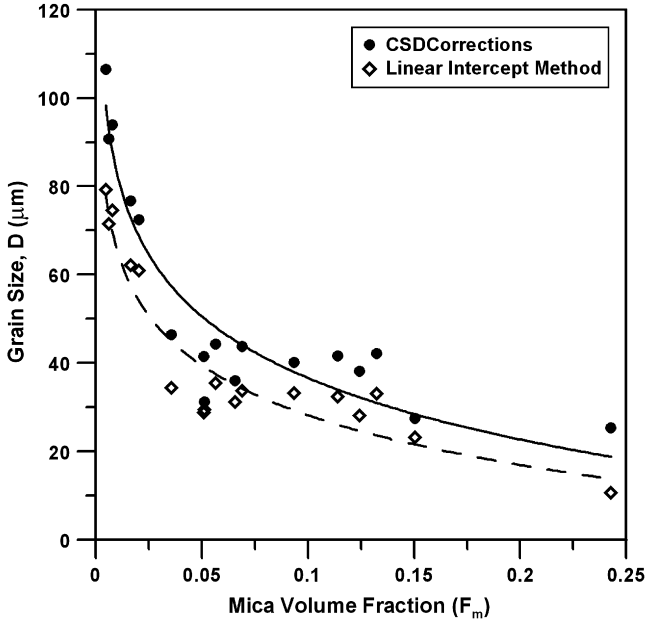

Fig. 5. Plot of average grain size of quartz against mica fraction in the quartz ribbons. Solid circle: average grain size measured from CSDCorrections 1.37 software (Higgins, 2000, 2006). Open diamond: average grain size from linear intercept method.

Table 1
Database of quartz–muscovite mylonite

Quartz ribbon	Mica volume %	Number of quartz grains measured	Average grain size of quartz (μm)		Average axial ratio of quartz in *b*-section (major/minor axis)	Number of mica grains measured	Average grain size of mica (μm)	Mica volume ratio (Boundary/Inclusion)
			CSDcorrections	Linear intercept				
13	0.47	101	106.54	79.28	1.51	58	9.05	1.45
16	0.61	107	90.69	71.47	1.62	139	6.82	1.54
12	0.79	98	93.91	74.60	1.57	54	9.98	3.13
15	1.64	104	76.69	62.25	1.41	154	8.27	2.90
14	2.02	187	72.40	61.04	1.42	359	7.54	2.89
18	3.56	108	46.44	34.39	1.53	372	5.55	6.54
17_re	5.08	73	41.52	28.88	1.55	239	6.03	6.83
03 + 04	5.11	264	31.17	29.46	1.47	582	5.96	1.74
11	5.64	131	44.33	35.45	1.35	634	5.53	2.48
05_2	6.55	110	36.06	31.22	1.47	273	6.68	8.76
10	6.90	125	43.79	33.74	1.48	363	6.93	5.11
06_re	9.35	88	40.21	33.22	1.43	288	6.38	7.10
07	11.39	119	41.65	32.43	1.54	244	8.15	8.95
08	12.44	117	38.21	28.20	1.56	292	7.34	14.48
09	13.24	129	42.24	33.16	1.65	336	8.18	12.85
02	15.04	109	27.53	23.28	1.64	170	7.26	11.13
01	24.28	80	25.40	10.65	2.00	59	9.17	12.46

mean grain size (Exner, 1972). As shown in Fig. 5, the mean grain sizes measured by the CSDCorrections 1.37 (Higgins, 2000, 2006) were 2–27 μm larger than those obtained from the linear intercept method.

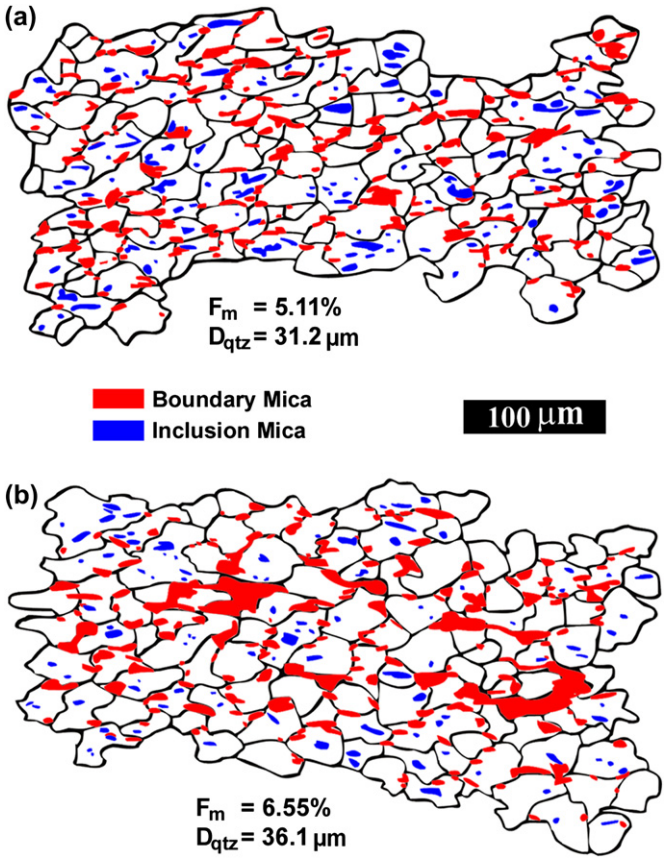

Fig. 6. Line drawing of quartz ribbons with mica fraction of (a) 5.11% and (b) 6.55%. F_m: mica fraction. D_{qtz}: mean grain size of quartz.

3.2. Lattice preferred orientation of quartz

The orientation of the quartz *c*-axes was measured using an automated fabric analyzer (Russell-Head and Wilson, 2001; Wilson et al., 2003). With a small fraction of mica, the quartz *c*-axis fabrics show a strong lattice preferred orientation of a Type-I crossed girdle pattern (Fig. 7; Lister et al., 1978). With a mica fraction of more than 3% however, the quartz grains show no strong lattice preferred orientation.

4. Discussion

4.1. Deformation mechanism

The microstructures and lattice preferred orientation of the quartz within the ribbons with a mica fraction of less than 3% indicate that the quartz grains were deformed by dislocation creep, with dynamic recovery mechanisms including grain boundary migration and subgrain rotation recrystallizations, corresponding to Regime 3 of Hirth and Tullis (1992) or subgrain rotation recrystallization/grain boundary migration recrystallization transition of Stipp et al. (2002a,b). For quartz grains in the almost pure quartz ribbon ($F_m < 1\%$), the paleostress was estimated to be 34–37 MPa, using the paleopiezometer of Twiss (1977) for a dynamically recrystallized grain size. For the paleostress estimation, the mean grain size of the quartz determined by the linear intercept method, as used by Twiss (1977), was employed. The paleopiezometer of Stipp and Tullis (2003) was also used to estimate the flow stress, which was found to be 22–25 MPa. Since Stipp and Tullis (2003) employed the root mean square diameter (e.g. Borradaile, 2003) for the grain size, the same method was used herein for the determination of the grain size. However, the applicability of the paleopiezometer of Stipp and Tullis (2003) to our mylonite is unclear, as they suggest the

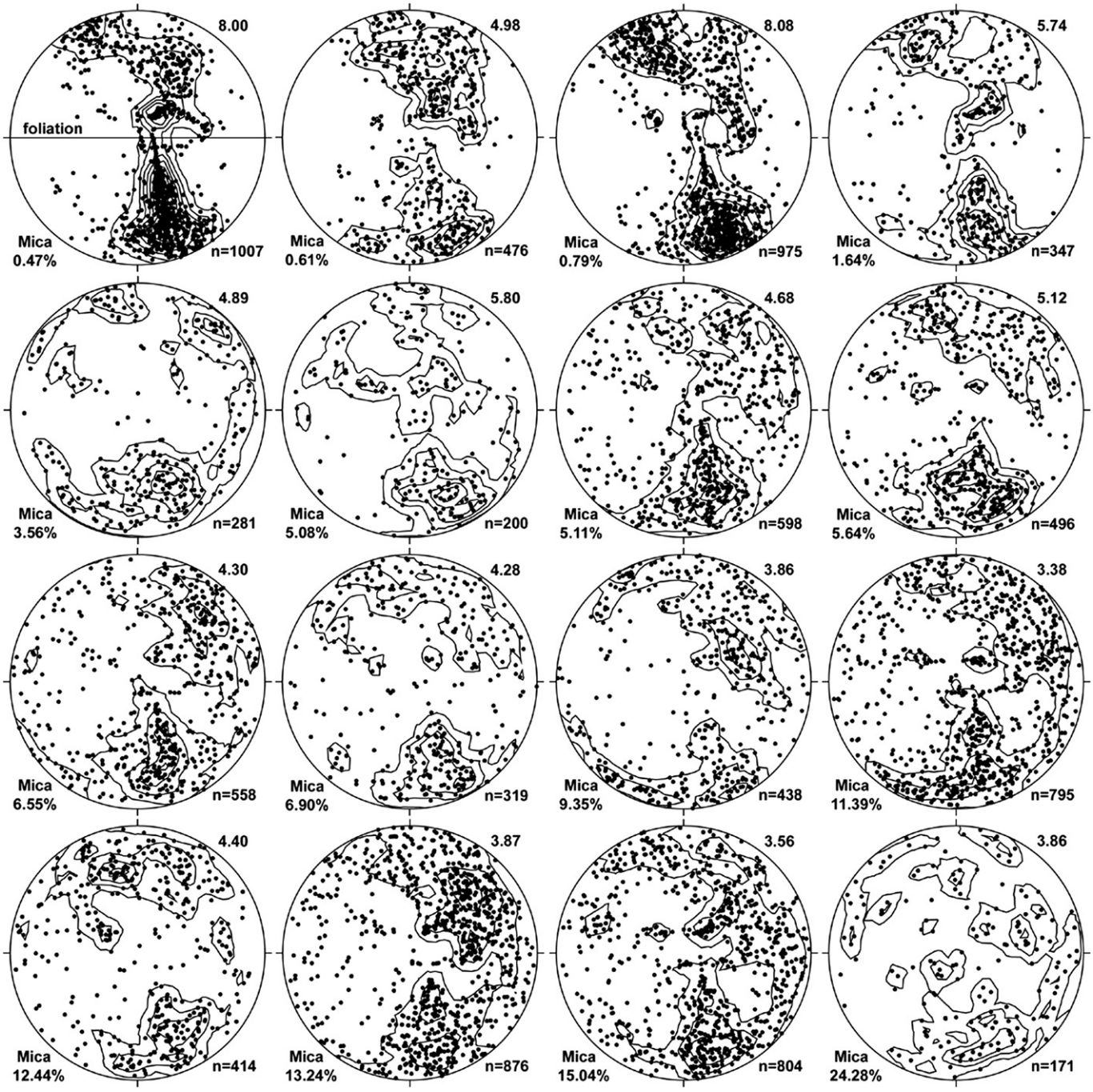

Fig. 7. *c*-Axis fabrics of quartz in the quartz ribbons with varying mica fraction. Equal-area, lower-hemisphere projection. Contour interval: 1% per 1% area. The number on the upper right of each stereogram represents the maximum density in %.

paleopiezometer for grain sizes of 3–45 μm, which are smaller than those (65–76 μm) of our pure quartz ribbon.

The paleostress and grain size data of the almost pure quartz ribbon were plotted on the deformation mechanism map of Etheridge and Wilkie (1979), assuming a deformation temperature of 450 °C (Fig. 8). Our data fall within the transition from dislocation creep to grain boundary sliding accommodated by dislocation creep. This is consistent with De Bresser et al.'s (2001) suggestion that dynamic recrystallization of a monophase aggregate results in a balance between grain size reduction and grain growth set up at the boundary between the dislocation creep field and grain-size sensitive creep field.

When the average grain size of quartz becomes less than 47 μm (35 μm by the linear intercept method), with a mica fraction of more than 3% in the ribbons, the quartz *c*-axes tend to have a weak or random orientation (see Fig. 7). The absence of a lattice preferred orientation suggests that the dominant deformation mechanism in the ribbons, with quartz grain sizes of 25–46 μm (11–34 μm by the linear intercept

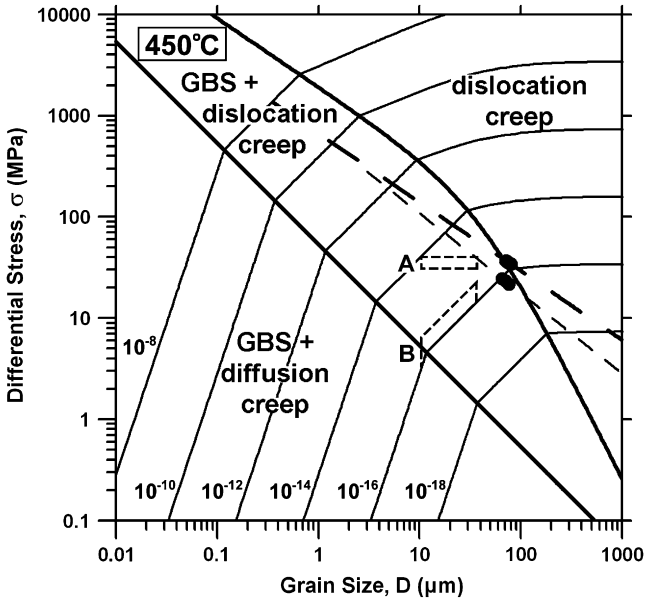

Fig. 8. Deformation mechanism map of quartz by Etheridge and Wilkie (1979), assuming the deformation temperature of 450 °C. Thick broken line: paleopiezometer of Twiss (1977). Thin broken line: paleopiezometer of Stipp and Tullis (2003). Solid circle: deformation condition of almost pure quartz ribbon. Box A: deformation condition of quartz ribbons with more than 3% mica fraction assuming equal differential stress. Box B: deformation condition of quartz ribbons with more than 3% mica fraction assuming equal strain rate.

method), may be grain boundary sliding, although independent evidence of grain boundary sliding is still required. If these quartz grain sizes are superimposed on the deformation mechanism map, assuming the same flow stress or the same strain rate as that of the almost pure quartz ribbon, they are within the regime of dominant grain boundary sliding accommodated by dislocation creep (Fig. 8). This is consistent with earlier suggestions that dominant grain boundary sliding would not be possible unless the grain size is stabilized below the steady-state recrystallized grain size due to the grain boundary pinning effect of second-phase particles (e.g. Etheridge and Wilkie, 1979; De Bresser et al., 2001).

The estimated strain rate of the almost pure quartz ribbon in the deformation mechanism map is about $10^{-16}\,s^{-1}$, which is much slower than those (10^{-14}–$10^{-12}\,s^{-1}$) inferred for natural shear zones (e.g. Pfiffner and Ramsay, 1982; Stipp et al., 2002b). One possible explanation for this discrepancy is that the muscovite-dominant matrix may have deformed at a faster strain rate while embedded quartz ribbons may have deformed at a slower strain rate. In other words, the bulk strain rate of the mylonite would have been faster than the local strain rate of the embedded quartz ribbons.

4.2. Particle dispersion

The dispersion of second-phase particles as well as their fraction affects the recrystallized grain size of the main phase (Figs. 5 and 6). Now the question is can the effect of the second-phase particle dispersion on the grain size of the recrystallized main phase be quantified? The quantification of the particle dispersion has long been attempted in ecology, with the most widely used method being that of 'distance-to-nearest-neighbor' (e.g. Clark and Evans, 1954). This method measures the degree to which the distribution of individual particles in a population for a given area departs from that of a random distribution. In other words, the ratio ('R' value) of the observed mean nearest-neighbor distance to the expected mean nearest-neighbor distance for an ideally random distribution is calculated, so that $R = 1$ for a random distribution, $0 \le R < 1$ for a clustered distribution (with $R = 0$ for the maximum clustering) and $1 < R \le 2.1491$ for a dispersed distribution (Clark and Evans, 1954). However, the effects of local aggregation, size, shape and shape-preferred-orientation of individual particles are not considered in the 'distance-to-nearest-neighbor' method. For example, clustered aggregates with a given fraction of particles can have the same R value as dispersed aggregates with the same particle fraction, but the dispersed aggregates will have a stronger pinning effect on the migrating boundaries of the main phase for a bulk rock volume (Fig. 9a). Also, rock volumes with different sizes, fractions and/or shapes of the second-phase particles can have the same R value, as long as the central points of the particles are in the same position (Fig. 9b).

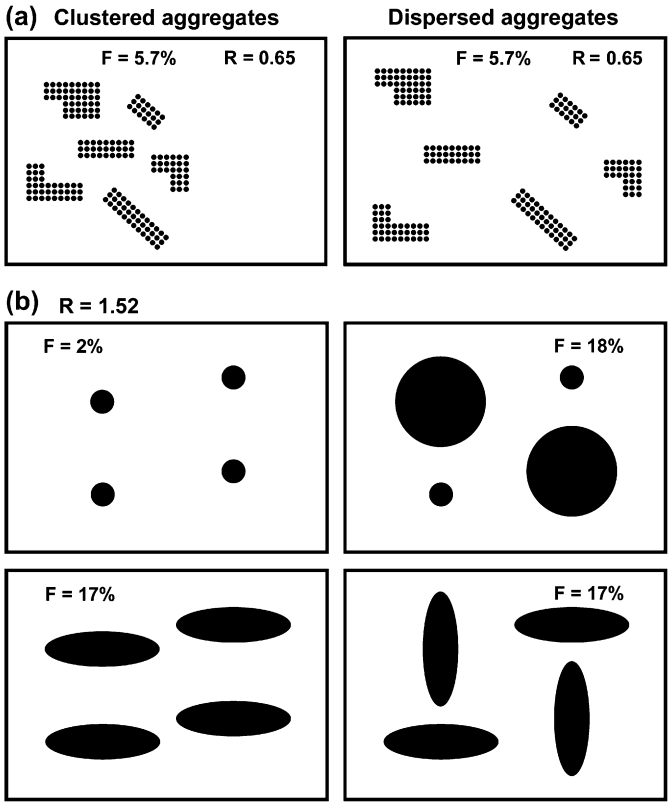

Fig. 9. Schematic diagrams of particle dispersion. (a) Clustered and dispersed aggregates with the same area fraction. (b) Dispersion of particles with different shapes and sizes but with the same R value. F: area fraction of particles.

Herwegh and Berger (2004) used the Zener parameter (ratio of size to volume fraction of second-phase particles) to quantify the effect of second-phase particle size and fraction on the size of the recrystallized main phase. A larger value of the Zener parameter corresponds to less effect of second-phase particles on the grain size of the main phase and vice versa in second-phase controlled microstructures. However, the Zener parameter can only be used when the second-phase particles have a dispersed distribution. For example, the Zener parameter ($\approx$117) for the ribbon with smaller size of quartz (Fig. 6a) is larger than that ($\approx$102) for the ribbon with larger size of quartz (Fig. 6b). Thus, for the quantification of the effect of the second-phase particle dispersion on the grain size of the recrystallized main phase, it is necessary to develop a new method, which not only considers the distance of the nearest neighbor, but also takes into account the local aggregation, size, shape and preferred orientation of individual particles.

5. Summary

(1) The grain size of dynamically recrystallized quartz in a quartz–muscovite mylonite markedly decreases, even with a small increase in the mica fraction. With a mica fraction of more than 3% however, the decrease in quartz grain size is retarded with further increases in the mica fraction.
(2) The dispersed distribution of mica has a more pinning effect on the migrating grain boundaries of quartz than the clustered distribution of mica.
(3) With a mica fraction of less than 3%, the dominant deformation mechanism of quartz grains (72–107 μm in average size) is dislocation creep. When the grain size of quartz becomes smaller than 47 μm, with a mica fraction of more than 3%, the dominant deformation mechanism of the quartz grains seems to switch to grain boundary sliding.

Acknowledgements

We appreciate the critical and constructive comments by reviewers Marco Herwegh and Janos Urai, and J. Hippertt's editorial advice. This work was supported by Korea Research Foundation grant C00435 (100699) and 2007 Korea University Research Grant to JHR.

References

Borradaile, G.J., 2003. Statistics of Earth Science Data. Springer-Verlag, Berlin, 351 pp.
Clark, P.J., Evans, F.C., 1954. Distance to nearest neighbor as a measure of spatial relationships in populations. Ecology 35, 445–453.
Cluzel, D., Lee, B.-J., Cadet, J.-P., 1991. Indosinian dextral ductile fault system and synkinemaic plutonism in the southwest of the Ogcheon belt (South Korea). Tectonophysics 194, 131–151.
De Bresser, J.H.P., Peach, C.J., Reijs, J.P.J., Spiers, C.J., 1998. On dynamic recrystallization during solid state flow: effects of stress and temperature. Geophysical Research Letters 25, 3457–3460.
De Bresser, J.H.P., Ter Heege, J.H., Spiers, C.J., 2001. Grain size reduction by dynamic recrystallization: can it result in major rheological weakening? International Journal of Earth Sciences 90, 28–45.
Etheridge, M.A., Wilkie, J.C., 1979. Grainsize reduction, grain boundary sliding and the flow strength of mylonites. Tectonophysics 58, 159–178.
Exner, H.E., 1972. Analysis of grain- and particle-size distributions in metallic materials. International Metallurgical Reviews 17, 25–42.
Heilbronner, R., Bruhn, D., 1998. The influence of three-dimensional grain size distributions on the rheology of polyphase rocks. Journal of Structural Geology 20 (6), 695–705.
Herwegh, M., Jenni, A., 2001. Granular flow in polymineralic rocks bearing sheet silicates: new evidence from natural examples. Tectonophysics 332 (3), 309–320.
Herwegh, M., Berger, A., 2004. Deformation mechanisms in second-phase affected microstructures and their energy balance. Journal of Structural Geology 26 (8), 1483–1498.
Herwegh, M., Berger, A., Ebert, A., 2005. Grain coarsening maps: a new tool to predict microfabric evolution of polymineralic rocks. Geology 33 (10), 801–804.
Higgins, M.D., 2000. Measurement of crystal size distributions. American Mineralogist 85, 1105–1116.
Higgins, M.D., 2006. Quantitative Textural Measurements in Igneous and Metamorphic Petrology. Cambridge University Press, 276 pp.
Hirth, G., Tullis, J., 1992. Dislocation creep regimes in quartz aggregates. Journal of Structural Geology 14 (2), 145–159.
Kim, J.H., Kee, W.S., 1994. Structural characteristics of the Soonchang shear zone, Korea. Journal of Southeast Asian Earth Sciences 9, 417–428.
Krabbendam, M., Urai, J.L., van Vliet, L.J., 2003. Grain size stabilisation by dispersed graphite in a high-grade quartz mylonite: an example from Naxos (Greece). Journal of Structural Geology 25 (6), 855–866.
Lister, G.S., Paterson, M.S., Hobbs, B.E., 1978. The simulation of fabric development in plastic deformation and its application to quartzite: the model. Tectonophysics 45, 107–158.
Mas, D.L., Crowley, P.D., 1996. The effect of second-phase particles on stable grain size in regionally metamorphosed polyphase calcite marbles. Journal of Metamorphic Geology 14, 155–162.
Masuda, T., Koike, T., Yuko, T., Morikawa, T., 1991. Discontinuous grain growth of quartz in metacherts: the influence of mica on a microstructural transition. Journal of Metamorphic Geology 9, 389–402.
Olgaard, D.L., 1990. The role of second phase in localizing deformations. In: Knipe, R.J., Rutter, E.H. (Eds.), Deformation Mechanisms, Rheology and Tectonics. Geological Society, London, Special Publications, vol. 54, pp. 175–181.
Olgaard, D.L., Evans, B., 1986. Effect of second-phase particles on grain growth in calcite. Journal of the American Ceramic Society 69, C-272–C-277.
Olgaard, D.L., Evans, B., 1988. Grain growth in synthetic marbles with added mica and water. Contributions to Mineralogy and Petrology 100, 246–260.
Panozzo, R.H., 1983. Two-dimensional analysis of shape-fabric using projections of digitized lines in a plane. Tectonophysics 95, 279–294.
Panozzo, R., 1984. Two-dimensional strain from the orientation of lines in a plane. Journal of Structural Geology 6 (1–2), 215–221.
Park, Y., Yoo, S.-H., Ree, J.-H., 2006. Weakening of deforming granitic rocks with layer development at middle crust. Journal of Structural Geology 28 (5), 919–928.
Pfiffner, O.A., Ramsay, J.G., 1982. Constraints on geological strain rates: arguments from finite strain states of naturally deformed rocks. Journal of Geophysical Research 87, 311–321.
Pryer, L.L., 1993. Microstructures in feldspars from a major crustal thrust zone: the Grenville Front, Ontario, Canada. Journal of Structural Geology 15 (1), 21–36.
Ree, J.-H., Hwang, S.-G., 1994. Indosinian dextral ductile fault system and synkinematic plutonism in the southwest of the Ogcheon belt (South Korea) – comment. Tectonophysics 230, 135–137.
Ree, J.-H., Kwon, S.-H., Park, Y., Kwon, S.-T., Park, S.-H., 2001. Pretectonic and posttectonic emplacements of the granitoids in the south central Okchon belt, South Korea: implications for the timing of strike-slip shearing and thrusting. Tectonics 20, 850–867.

Ree, J.-H., Kim, H.S., Han, R., Jung, H., 2005. Grain-size reduction of feldspars by fracturing and neocrystallization in a low-grade granitic mylonite and its rheological effect. Tectonophysics 407 (3–4), 227–237.

Russell-Head, D.S., Wilson, C.J.L., 2001. Automated fabric analyzer system for quartz and ice. Geological Society of Australia Abstracts 64, 159.

Sagong, H., Kwon, S.-T., Ree, J.-H., 2005. Mesozoic episodic magmatism in South Korea and its tectonic implication. Tectonics 24, doi:10.1029/2004TC001720. TC5002.

Sander, B., 1970. An Introduction to the Study of Fabrics of Geological Bodies. (Phillips, F.C., Windsor, G., translators of a 1950 publication in German). Pergamon Press, 641 pp.

Stipp, M., Stünitz, H., Heilbronner, R., Schmid, S.M., 2002a. The eastern Tonale fault zone: a 'natural laboratory' for crystal plastic deformation of quartz over a temperature range from 250 to 700°. Journal of Structural Geology 24 (12), 1861–1884.

Stipp, M., Stünitz, H., Heilbronner, R., Schmid, S.M., 2002b. Dynamic recrystallization of quartz: correlation between natural and experimental conditions. In: de Meer, S., Drury, M.R., de Bresser, J.H.P., Pennock, G.M. (Eds.), Deformation Mechanisms, Rheology and Tectonics: Current Status and Future Perspectives. Geological Society, London, Special Publications, vol. 200, pp. 171–190.

Stipp, M., Tullis, J., 2003. The recrystallized grain size piezometer for quartz. Geophysical Research Letters 30 (21), doi:10.1029/2003GL018444. SDE 3.

Twiss, R.J., 1977. Theory and applicability of a recrystallized grain size paleopiezometer. Pageoph 115, 227–244.

Wilson, C.J.L., Russell-Head, D.S., Sim, H.M., 2003. The application of an automated fabric analyzer system to the textural evolution of folded ice layers in shear zones. Annals of Glaciology 37, 7–17.

Yanai, S., Park, B.-S., Otoh, S., 1985. The Honam shear zone (South Korea): deformation and tectonic implication in the Far East. Scientific Papers of the College of Arts and Sciences, University of Tokyo, vol. 35, pp. 181–210.